

# CMOS-compatible broadband co-propagative stationary Fourier transform spectrometer integrated on a silicon nitride photonics platform

XIAOMIN NIE,<sup>1,2,\*</sup> EVA RYCKEBOER,<sup>1,2</sup> GUNTHER ROELKENS,<sup>1,2</sup> AND ROEL BAETS<sup>1,2</sup>

<sup>1</sup>Photonics Research Group, Department of Information Technology, Ghent University-imec, Ghent B-9000, Belgium

<sup>2</sup>Center for Nano- and Biophotonics(NB-Photonics), Ghent University, Ghent B-9000, Belgium

\*e-mail: Xiaomin.Nie@ugent.be

**Abstract:** We demonstrate a novel type of Fourier Transform Spectrometer (FTS) that can be realized with CMOS compatible fabrication techniques. This FTS contains no moving components and is based on the direct detection of the interferogram generated by the interference of the evanescent fields of two co-propagating waveguide modes. The theoretical analysis indicates that this type of FTS inherently has a large bandwidth (>100 nm). The first prototype that is integrated on a  $Si_3N_4$  waveguide platform is demonstrated and has an extremely small size ( $0.1\text{ mm}^2$ ). We introduce the operation principle and report on the preliminary experiments. The results show a moderately high resolution (6 nm) which is in good agreement with the theoretical prediction.

© 2017 Optical Society of America

**OCIS codes:** (300.6300) Spectroscopy, Fourier transforms, (300.6190) Spectrometers, (130.3120) Integrated optics devices.

## References and links

1. P. R. Griffiths and J. A. De Haseth, *Fourier Transform Infrared Spectrometry* (John Wiley and Sons, 2007).
2. C. P. Bacon, Y. Mattley, and R. DeFrece, "Miniature spectroscopic instrumentation: applications to biology and chemistry," *Rev. Sci. Instrum.* **75**(1), 1–16 (2004).
3. T. Sandner, A. Kenda, C. Drabe, H. Schenk, and W. Scherf, "Miniaturized FTIR-spectrometer based on optical MEMS translatory actuator," in *MOEMS-MEMS 2007 Micro and Nanofabrication* (ISOP, 2007), paper 646602.
4. K. Yu, D. Lee, U. Krishnamoorthy, N. Park, and O. Solgaard, "Micromachined Fourier transform spectrometer on silicon optical bench platform," *Sens. Actuators A: Phys.* **130**, 523–530 (2006).
5. L. Wu, A. Pais, S. R. Samuelson, S. Guo, and H. Xie, "A mirror-tilt-insensitive Fourier transform spectrometer based on a large vertical displacement micromirror with dual reflective surface," in *TRANSDUCERS 2009-2009 International Solid-State Sensors* (IEEE, 2009), pp. 2090–2093.
6. E. Le Coarer, S. Blaize, P. Benech, I. Stefanon, A. Morand, G. Lérondel, G. Leblond, P. Kern, J. M. Fedeli, and P. Royer, "Wavelength-scale stationary-wave integrated Fourier-transform spectrometry," *Nat. Photonics* **1**(8), 473–478 (2007).
7. M. Florjańczyk, P. Cheben, S. Janz, A. Scott, B. Solheim, and D.X. Xu, "Planar waveguide spatial heterodyne spectrometer," *Proc. SPIE* **6796**, 67963J (2007).
8. S. P. Davis, M. C. Abrams, and J. W. Brault, *Fourier Transform Spectrometry* (Academic Press, 2001).
9. X. Nie, E. Ryckeboer, G. Roelkens, and R. Baets, "Novel concept for a broadband co-propagative stationary Fourier transform spectrometer integrated on a  $Si_3N_4$  waveguide platform," in *Conference on Lasers and Electro-Optics*, OSA Technical Digest (online) (Optical Society of America, 2016), paper JW2A.120.
10. K. Sohelmainen, M. Kapulainen, M. Harjanne, and T. Aalto, "Adiabatic and multimode interference couplers on silicon-on-insulator," *IEEE Photonics Technol. Lett.* **18**(21), 2287–2289 (2006).
11. W. Shi, X. Wang, W. Zhang, L. Chrostowski, and N.A.F. Jaeger, "Contradirectional couplers in silicon-on-insulator rib waveguides," *Opt. Lett.* **36**(20), 3999–4001 (2011).
12. A.Z. Subramanian, P. Neutens, A. Dhakal, R. Jansen, T. Claes, X. Rottenberg, F. Peyskens, S. Selvaraja, P. Helin, B. Du Bois, and K. Leyssens, "Low-loss singlemode PECVD silicon nitride photonic wire waveguides for 532-900 nm wavelength window fabricated within a CMOS pilot line," *IEEE Photonics J.* **5**(6), 2202809 (2013).
13. M. Fiers, E. Lambert, S. Pathak, B. Maes, P. Bienstman, W. Bogaerts, and P. Dumon, "Improving the design cycle for nanophotonic components," *J. Comput. Sci.* **4**(5), 313–324 (2013).

14. F. Thomas, B. Martin, C. Duchemin, R. Puget, E. Morino, C. Bonneville, T. Gonthize, P. Benech and E. Le Coarer, "Major advances in developments and algorithms of the stationary-wave integrated Fourier-transform technology," in *Light, Energy and the Environment*, OSA Technical Digest (online) (Optical Society of America, 2016), paper FTh2C.2.
15. A. Dhakal, P. Wuytens, F. Peyskens, A. Z. Subramanian, A. Skirtach, N. Le Thomas, and R. Baets, "Nanophotonic Lab-On-A-Chip Raman sensors: a sensitivity comparison with confocal Raman microscope," in *Proceedings of IEEE Conference on BioPhotonics* (IEEE, 2015), pp. 1–4.
16. E. Ryckeboer, R. Bockstaele, M. Vanslembrouck, and R. Baets, "Glucose sensing by waveguide-based absorption spectroscopy on a silicon chip," *Biomed. Opt. Express* 5(5), 1636-1648 (2014).

## 1. Introduction

Optical spectrometers have become an indispensable tool in various fields that involve optical spectrum analysis. Its application ranges from biochemical sensing to food quality control and even to astronomical radiation analysis. Among all types of modern spectrometers, the Fourier transform infrared spectrometer (FTIR or FTS) offers important advantages such as a high throughput and the multiplex advantages [1]. In a standard FTIR, all wavelengths are measured simultaneously in a large series of subsequent increments of the optical path difference (OPD) in a Michelson interferometer. The spectral content of the signal is encoded in the interferogram, created by the interference between an optical signal and its delayed version, and can be decoded by applying a Fourier transform. Typically, the longer the interferogram an FTS can measure, the higher the spectral resolution.

The high demand for optical spectrometers and the growing preference for portable and robust devices have together created a trend towards the miniaturization and integration of the FTS [2]. Although there exist various miniaturized Fourier transform spectrometers that still involve moving components [3–5], it would be better to have an FTS without any moving components. Currently, integrated FTS that are implemented without any moving components can be divided mainly into two categories: the stationary wave integrated FTS (SWIFTS) [6] and the spatial heterodyne spectrometer (SHS) [7].

In the scheme of SHS, an array of unbalanced Mach-Zehnder interferometers (MZIs) is used to generate a spatially varying interference pattern. To increase the resolution for a given spectral bandwidth, a larger number of MZIs is required [7], implying a rapidly growing size of the device when scaling the spectral resolution. However, for applications that have less constraints on the footprint, SHS can be particularly suitable since the underlying principle allows SHS to achieve high resolution in a narrow spectral band without degrading the signal to noise ratio.

On the other hand, SWIFTS-based devices can achieve high resolution within a small footprint. In such devices, the interferogram is the standing wave pattern generated by the interference of two counter-propagating beams inside a waveguide. On top of the waveguide, nano-scatterers are carefully positioned to couple this interference pattern to a detector array. As introduced in the work of Etienne le Coarer et al [6], the pitch of the interference pattern can be expressed as  $\lambda/(2n_{eff})$  which is much smaller than the pitch size of state-of-the-art photodiode arrays. As a result, the interferogram is subsampled, leading to a limitation on the spectral bandwidth of the FTS.

In this paper, we propose a new type of stationary wave integrated FTS design. Our proposed design, as a waveguide based stationary FTS, is compact and stable. Moreover, in our design, the subsampling is avoided by generating an interferogram that is spatially stretched compared to the original SWIFTS concept. This effectively helps to lift the restriction on the operation bandwidth. Our spectrometer is designed to target on-chip Raman or absorption spectroscopy applications. The envisioned bandwidth of about 100 nm is large enough to accommodate these applications. Compared to a SWIFTS, for a given device length, a lower resolution is obtained in our case. However, we demonstrate that a spectral resolution of 6 nm can be realized, which is sufficient for most applications of Raman spectroscopy and infrared absorption spectroscopy of

liquids and solids. Since in on-chip Raman or infrared absorption spectroscopy the signals are collected in a single mode waveguide, the use of single mode waveguides in the spectrometer does not impair the light collection efficiency of the spectrometer.

We have developed a first prototype that is fabricated on a CMOS compatible  $Si_3N_4$  waveguide platform. This photonic integrated circuit (PIC) technology allows to fabricate spectrometers cost-effectively at a wafer scale with high yield. Moreover, the FTS prototype can be further integrated with a CMOS photodiode array to create a very compact, portable device.

In the following sections, we will first introduce the theoretical principles of our new device and discuss the design and simulation results. After that, we will give the first experimental results from our prototype on-chip FTS. We will discuss these preliminary experimental results and analyze the potential of our device.

## 2. Principle of the co-propagative stationary FTS

All types of Fourier transform spectrometers are based on the creation of an optical interferogram. In the co-propagative Stationary FTS that is proposed here, the interferogram is generated by the interference between two waveguide modes that propagate in the same direction but with a slightly different phase velocity. This is the origin of the name co-propagative stationary FTS. A 3D representation of the structure we propose is shown in Fig. 1.

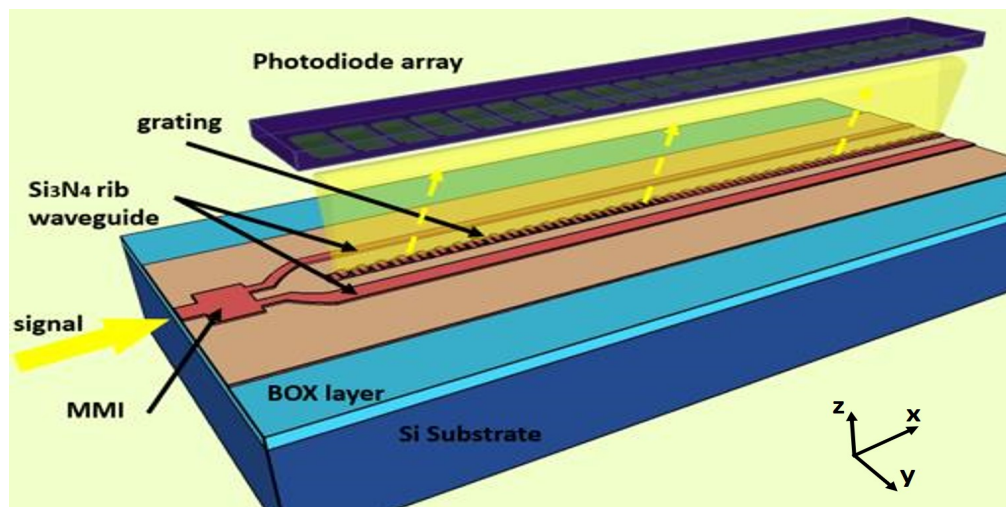


Fig. 1. Conceptual drawing of the co-propagative stationary FTS. [9]

The signal to be analyzed is first injected into the input port of a Multimode Interference (MMI) coupler which then splits the light into two parallel waveguides with different width. One can also understand this as the excitation of two supermodes in a coupled waveguide system. These two modes are predominantly confined in the left and right waveguide core and are orthogonal to each other so that there will be no energy exchange related to mode conversion along the propagation. The excited waveguide modes that propagate in the waveguides with different widths will have different phase velocities. We space the parallel waveguides in such a way that the evanescent tails of the two waveguide modes slightly overlap. In this way, the interferogram is created in the region between the two parallel waveguides. At the location where the interferogram has the best contrast, a well-designed grating with proper period is positioned in order to diffract the interferogram upwards onto the detection system, for example,

a photodiode array as shown in Fig. 1.

As an example, we consider the injection of a monochromatic signal with a wavelength  $\lambda$ . The intensity distribution of the interferogram  $I$  as a function of propagation distance  $x$  can be related to the optical intensity in each waveguide as

$$I(x) \propto I_1 + I_2 + 2\sqrt{I_1 I_2} \cos(\Delta\beta x), \quad (1)$$

with  $I_{1,2}$  the intensity of the individual waveguide mode and  $\Delta\beta$  the propagation constant difference, which is in approximation proportional to the difference in the effective indices of the two waveguide modes  $\Delta n_{eff}$ ,

$$\Delta\beta = \beta_1 - \beta_2 \approx 2\pi \frac{\Delta n_{eff}}{\lambda}. \quad (2)$$

As a result, we can express the period of the interferogram as

$$\Lambda = \frac{\lambda}{\Delta n_{eff}}. \quad (3)$$

If one compares this expression to what is found in the original SWIFTS design [6], one can find that we are actually stretching the interferogram by a factor of  $2n_{eff}/\Delta n_{eff}$ , which makes the period as large as several tens of micrometers. Consequently, it is now easy to find photodiode arrays that are commercially available and that have a pixel pitch small enough to avoid subsampling of the interferogram.

One of the key characteristics of the FTS is the spectral resolution. In our co-propagative stationary FTS, the spectral resolution is determined by the length of the single-sided interferogram that we capture. To give the expression of the resolution, we consider a single wavelength injection. The fact that the interferogram we can measure only covers a finite length  $L$  will broaden the delta-shaped spectrum in the Fourier domain into a sinc line shape,  $\text{sinc}[\pi(f_z - 1/\Lambda)L]$ , where  $f_z$  is the spatial frequency. We define the spectral resolution, which equals to the Full Width Half Maximum (FWHM) of the sinc shape spectrum, as

$$\delta\lambda \approx 1.207 \frac{\lambda^2}{\Delta n_{eff} L}. \quad (4)$$

In principle, one can obtain higher spectral resolution through additional data processing [8]. However, as this topic is out of scope for this paper, we will continue to use the resolution as defined by Eq. (4) in the following discussions. Now, if we for example assume an effective index difference of 0.05 at the wavelength of 800 nm, which is practical in a  $Si_3N_4$  rib waveguide platform, and consider a 1 cm long interferogram, we can expect a spectral resolution of 1.28 nm. According to Eq. (4), the resolution can be improved by simply making the waveguide longer and thus recording a longer interferogram.

Although Eq. (4) gives the achievable spectral resolution, other factors can also lower the resolution in practice. An important one is that as we need to constantly couple power to the detector, an exponential decay will be superimposed on the interferogram, which leads to line broadening and lower resolution. In principle, one can carefully design a grating with increasing strength to partially compensate the power decay and thus approach the resolution expressed by Eq. (4). However, in this first prototype, a uniform grating is designed which leads to a lower resolution as we will see later in the experimental results. The exponential decay superimposed on the interferogram will also degrade the dynamic range of the system, as the optical intensity of the interferogram at large OPD is reduced. To allow the system to have the same dynamic range as in a standard FTS, we will try to improve the compensation of the exponential decay in future versions of the design.

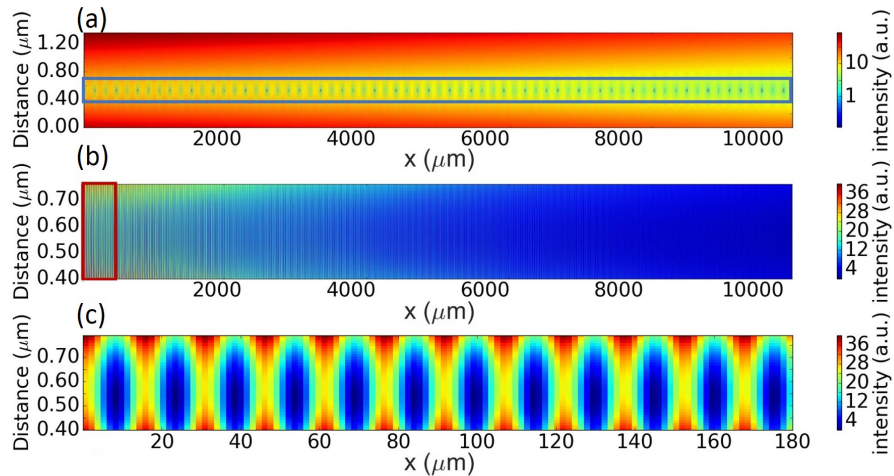


Fig. 2. (a) Simulation results of the interference pattern between the two waveguides in the case of single wavelength injection. The position where one should position the grating is marked by the blue frame. (b) A zoom in of the interferogram in the grating region. (c) A zoom-in of the first several periods of the intensity oscillation. [9]

Another characteristic is the operational spectral range. Since we stretch the interferogram and make its intensity oscillation period as large as a few tens of micrometers, we can fulfill Nyquist-Shannon's sampling theorem and avoid subsampling. Now the only factors that limit the bandwidth are the operation wavelength range of the detectors and the spectral range in which the waveguides remain single-mode, which is typically a few hundreds of nanometers in the  $Si_3N_4$  platform. In this design, the bandwidth is limited by the MMI coupler to around 100 nm which is already sufficient for some on-chip spectroscopy applications. However, in future versions of the design, we can extend the bandwidth by exploring alternative splitters [10].

Last but not least, it is important to have a proper design of the grating that we want to position between the two parallel waveguides. Since the purpose of the grating is to diffract the interferogram onto the detector array, it determines the efficiency of the spectrometer. In the design of the first prototype, we use a standard grating, which diffracts only half of the power in the grating region upwards. However, for future versions of the design, we have learned from our ongoing research program that a carefully designed high directionality grating can diffract more than half of the power upwards and thus lead to a higher efficiency. Moreover it should have very weak reflections, minimizing contra-directional coupling between the two waveguides [11]. This will help reduce the distortions of the interferogram to be measured. The grating strength and the distances between the waveguides and the grating will together play an important role to determine the quality of the interferogram that we can measure. In Fig. 2, we show the simulation result of the optical intensity distribution in the region between the two waveguides, assuming the injected signal is monochromatic. The blue frame in Fig. 2(a) indicates that the grating should be positioned at the region where the optical intensity of the evanescent fields of both waveguide modes have the same strength, which leads to best contrast.

### 3. Fabrication of the first prototype

To realize the first prototype of the co-propagative stationary FTS, we used the CMOS pilot line of IMEC [12]. The fabrication starts with a bare silicon wafer. In the first step, a layer of silicon dioxide is deposited using a high-density plasma (HDP) chemical vapor deposition

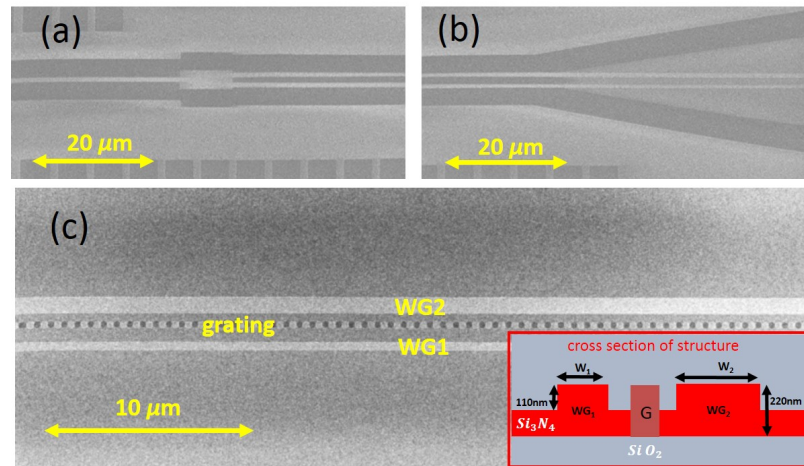


Fig. 3. SEM pictures of: (a) Fully etched MMI, (b) taper section tapering wire waveguides to rib waveguides with different widths, (c) the main structure containing two rib waveguides with different widths and a grating. The insert in (c) shows the cross section, with G indicating the grating.

(CVD) process. Then, on top of the 2200 nm  $SiO_2$  layer,  $Si_3N_4$  is deposited using Plasma-Enhanced Chemical Vapor Deposition (PECVD). The thickness of  $Si_3N_4$  was chosen to be 220 nm for 780 to 900 nm wavelength operation. After that, the wafers are patterned by deep UV lithography with a shallow (110 nm) and full (220 nm) etch with the minimum feature size of 150 nm. The device design is created with the commercial design software IPKISS.flow [13].

Scanning Electron Microscope (SEM) views of our device are shown in Fig. 3. In Fig. 3(a), we show the fully etched MMI, which is used to split the input signal into two wire waveguides with an equal splitting ratio (50:50). After that, the waveguides are tapered to rib waveguides with different widths in the tapering section as shown in Fig. 3(b). A small part of the main structure, including two rib waveguides with different widths and a grating in between is shown in Fig. 3(c) with an insert sketching the cross section. The total length of the grating goes up to 7500  $\mu m$  with a period of 640 nm, allowing the near-vertical diffraction for a broad wavelength range at a center wavelength of 850 nm. The overall footprint of the single co-propagative stationary FTS is very small ( $\sim 0.1 \text{ mm}^2$ ), offering the potential of integrating multiple FTS devices on a single  $Si_3N_4$  die. This could be useful for example in hyperspectral imaging with high spectral resolution.

#### 4. Preliminary experiments and discussion

In the experiments, we use two lasers to provide clear input spectral features. As shown in Fig. 4(a), the two lasers which are used in the experiments include an ultra narrow linewidth CW Ti:Sapphire laser from M2lasers (710-975 nm) and a TLB-6318 tunable laser from Newport (890-910 nm). Both are followed by a polarization controller (PC) to allow independent polarization tuning. A 50:50 combiner is then applied to combine the two lasers. After proper alignment, the signal is horizontally coupled into our device by a lensed fiber (LF). For detection, instead of using a detector array in proximity to the SiN chip to measure the interferogram, we use a microscope objective lens (OBJ) to image the interferogram onto a CCD camera. Since the imaging system, i.e. the objective lens combined with the CCD camera, has a limited field of view which is much smaller than the dimension of the interferogram, we need to scan it along the direction parallel to the grating to cover the whole interferogram. Therefore, to reconstruct the complete interferogram, we need to take several snapshots during the scanning and afterwards

stitch them together.

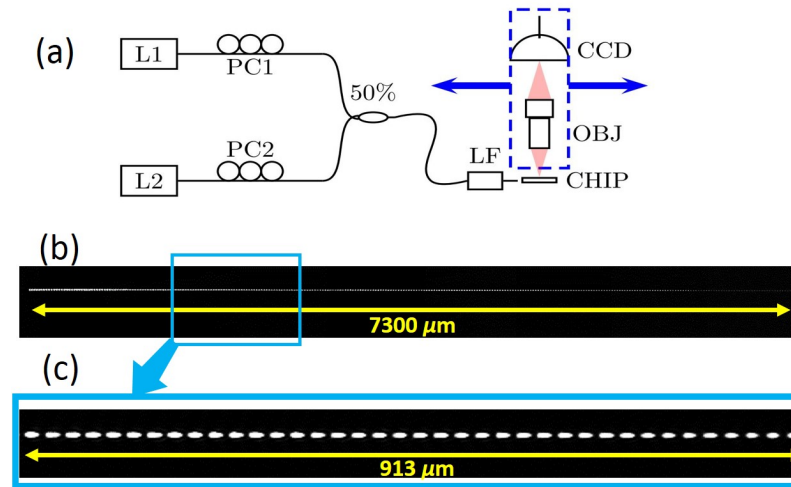


Fig. 4. (a) The setup used in the preliminary experiments, where we use a lensed fiber (LF) to couple the signal into the chip, and project the interferogram onto a CCD camera with an objective lens (OBJ). Two laser sources (L1 and L2) with the polarization controller (PC) can be applied simultaneously or individually. The CCD camera and OBJ (both shown inside the blue dash box) can move together to scan the whole interferogram. (b) The entire interferogram reconstructed by stitching of 8 snapshots. (c) One of the snapshots obtained during the scanning.

In one of the measurements, we first consider the input from one of the two lasers. The interferogram obtained from the monochromatic signal at 895 nm is shown in Figs. 4(b) and 4(c), where one can clearly see a periodic bright-to-dark pattern.

From the snapshots, we can then extract the intensity profile of the interferogram, as shown in Fig. 5(a). From this profile, one can clearly observe an exponential decay of the interferogram as expected. In order to decode the spectral content of the injected signal from the interferogram, we use the Fast Fourier Transform (FFT) function in Matlab to process the raw data. After the Fourier transform processing, the resulting spectrum is mapped onto the wavelength axis by choosing a proper  $\Delta n_{eff}$ , i.e. the difference in effective index. With  $\Delta n_{eff}$  of 0.0376 which is not far away from the simulation value 0.0387, we can match the position of the peak with the known laser source wavelength as shown in Fig. 5(b).

Once we know the value of  $\Delta n_{eff}$ , we can theoretically calculate the resolution to be 3.5 nm from Eq. (4). However, the FWHM of the main peak in Fig. 5(b) is measured to be around 6 nm. To investigate the broadening, we calculated the Fourier transform of a perfect sinusoidal interferogram with the same period for two cases. These perfect sinusoidal lines are shown in the inset of Fig. 5(a) for the case (in green) that there is no power decay along the length of the device and for the case (in red) where the same decay rate as in the measured interferogram is considered. The resulting spectra with the same color code are plotted in Fig. 5(c). The theoretical 3.5 nm FWHM is observed for the green spectrum while the red one has a FWHM of 5.5 nm. This leads to the conclusion that the broadening is mainly resulting from the exponential decay that is superimposed on the sinusoidal interferogram pattern.

We also tested our device with two spectral lines. In Fig. 6, we present two sets of experimental results, each including the stitched intensity profile of the interferogram, the calculated spectrum and one of the snapshots taken by the CCD camera. Figures 6(a) and 6(b) show the interferogram and spectrum generated by the lasers tuned to 822 nm and 900 nm while

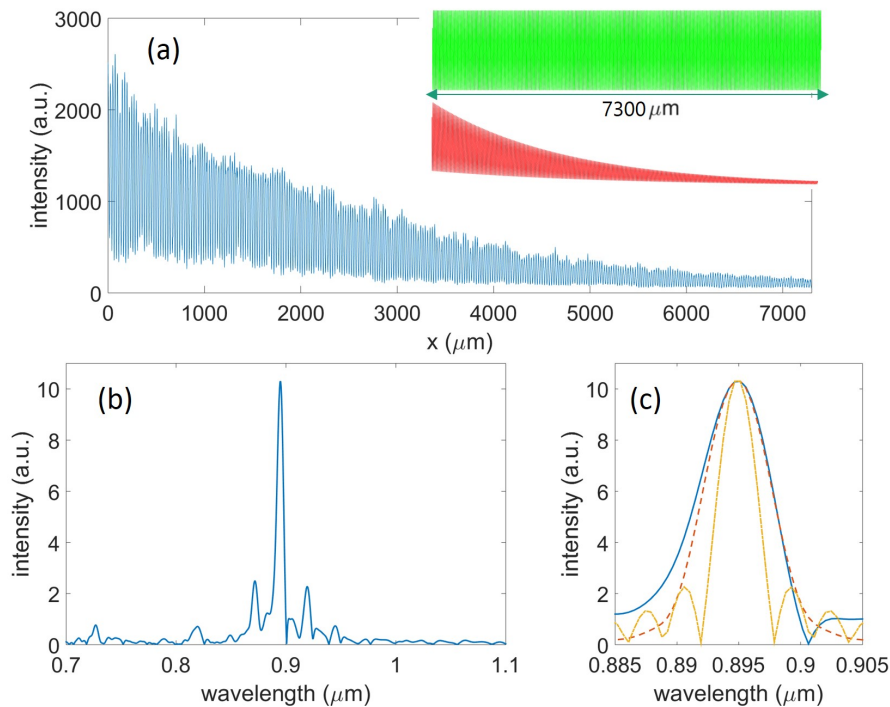


Fig. 5. (a) Plot of the intensity profile extracted from the measured interferogram. The inset shows the computed sinusoidal interferogram with same period and total length as the measured one: the red curve has the same power decay rate while the green curve has no decay. (b) The spectrum calculated from the interferogram measured as shown in (a). (c) A zoom-in of the spectrum displayed in (b) together with the green and red spectrum resulting from the Fourier transform of the calculated interferogram in the inset of (a).

Figs. 6(c) and 6(d) are from 876 nm and 900 nm laser light.

To get the spectra shown in Fig. 6, we followed a different procedure compared to the previous experiment. Instead of applying an FFT directly to the raw data, we first smooth the raw data using a 9-point moving average function in Matlab, which replaces the value at a certain point with the average of the values of the surrounding 9 points. After that we calculate the FFT of the smoothed data.

So far, we demonstrated the performance of our on-chip co-propagative stationary FTS in both monochromatic and polychromatic cases. The results are promising and in good agreement with the theoretical prediction. However, some unexpected small spectral features do exist in all of the spectra we obtained. The unexpected bumps can be attributed to the various distortions of the interferogram.

Part of the distortions originate in the fabrication uncertainty that is inherent to patterning small features in the grating. Fabrication defects in the grating units can lead to local changes of the diffraction strength, which generate bumps in the interferogram. To deal with this type of distortion, one can apply a smoothing function to the raw data. By comparing the spectra in Fig. 6 to the one in Fig. 5, one can find that the side lobes are clearly suppressed after applying the smoothing function.

In order to obtain a resolution closer to the theoretical value, several approaches can be followed. One way would be to calibrate the devices after design and fabrication. Once the decay rate for a certain device is known, one can compensate and remove the decay by data processing. Recent research has demonstrated that more sophisticated data processing such as

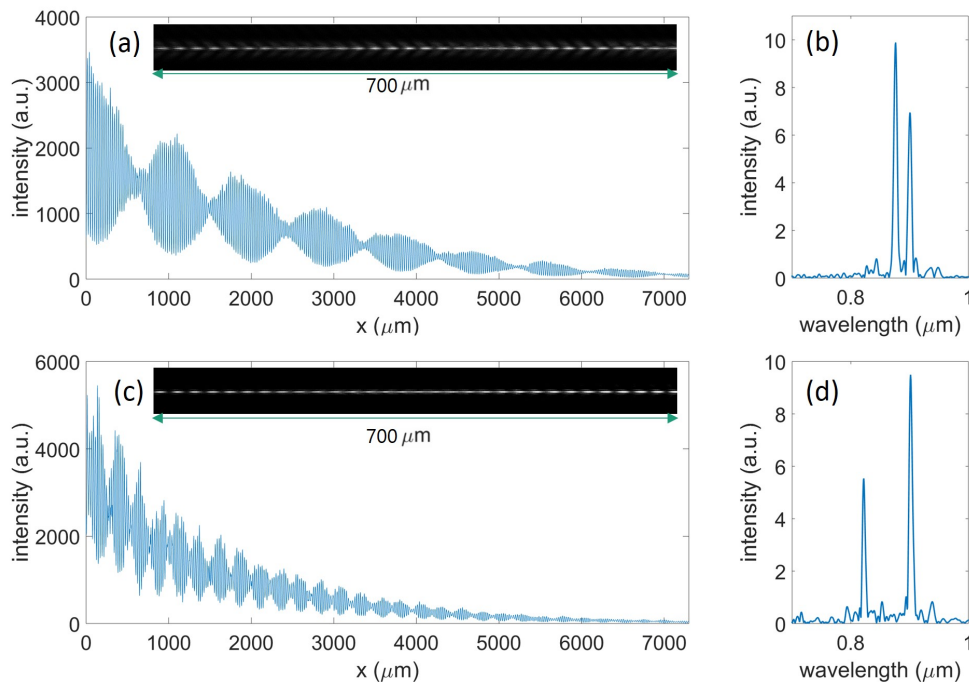


Fig. 6. Two sets of experimental results obtained with two laser sources. The interferogram (a) and the spectrum (b) of the input laser light of 900 nm & 822 nm. The interferogram (c) and the spectrum (d) for 900 nm & 876 nm laser light. The insets show the snapshots taken by the CCD camera.

calibrating the device to correct the raw data and optimizing the Fourier Transform algorithm can significantly improve the performance of this type of FTS [14]. However, one should keep in mind that data processing will inevitably amplify the high frequency noise to some extent as the signal to noise ratio degrades at larger OPD. Therefore a better solution would come from a design point of view. For example, a carefully designed apodized grating with increasing grating strength and/or the waveguides that have decreasing separation can lead to an improved compensation of the exponential decay in future versions of the design.

Some other distortions result from our measurement method. On the one hand, since the imaging system has a certain degree of non-uniformity in magnification over the entire field of view, we observe a slightly varying pitch in the interferogram in every snapshot. On the other hand, as we are stitching several snapshots to obtain the complete interferogram, there can be some discontinuities at the stitching positions.

Besides, the current imaging system also sets a limitation on the operation bandwidth. Because of the chromatic aberration of the objective lens, we cannot focus all the light in a broad wavelength band simultaneously onto the CCD camera. In the experiments of dual-wavelength injection, we found it very hard to get a clear interferogram when the two wavelengths are separated by more than 80 nm.

In future work, we will move to proximity measurements, where we flip-chip a bare detector array chip such as a CCD line scanner chip and position it very close ( $<100 \mu\text{m}$ ) to the silicon nitride chip that contains our device. It is obvious that in this way the distortions associated with the imaging system will no longer be there. By choosing a sensor chip with a high pixel count, we don't need to scan the interferogram, thus we avoid the distortions associated with image

stitching. Some other efforts will be dedicated to the development of an optimization algorithm that can automatically correct the distortions associated with the fabrication defects.

## 5. Conclusion

In this paper, we proposed a new type of integrated stationary FTS that is based on the interference between the evanescent fields of two co-propagating waveguide modes. We tested the first prototype that is fabricated on a  $Si_3N_4$  waveguide platform with CMOS compatible technologies. The preliminary experimental results for both monochromatic and polychromatic operation are presented and are in good agreement with the theoretical expectations. We also discussed the problems of the current prototype and measurement set-up, which provides guidelines to further improve the performance of our device. Nevertheless, we believe that the co-propagative stationary FTS we proposed in this paper can be a promising candidate for a compact and robust on-chip spectrometer since it provides moderately high resolution over a broad wavelength range in a very small area without any moving components. Although the prototype demonstrated in this paper is designed for the operation in the near infrared region, this FTS can also be designed for other wavelength windows that sit in the transparency wavelength range of the waveguide. Taking into account all its unique properties, we believe that our proposed co-propagative stationary FTS is suitable for further integration into various lab-on-a-chip systems such as on-chip Raman or absorption spectroscopy systems [15, 16].

## Funding

ERC-InSpectra Advanced Grant; European Horizon 2020 PIX4life Project.

## Acknowledgments

The authors thank Yunpeng Zhu, Ghent University-imec, for helping with the SEM pictures.